

Provided for non-commercial research and education use.  
Not for reproduction, distribution or commercial use.



This article appeared in a journal published by Elsevier. The attached copy is furnished to the author for internal non-commercial research and education use, including for instruction at the authors institution and sharing with colleagues.

Other uses, including reproduction and distribution, or selling or licensing copies, or posting to personal, institutional or third party websites are prohibited.

In most cases authors are permitted to post their version of the article (e.g. in Word or Tex form) to their personal website or institutional repository. Authors requiring further information regarding Elsevier's archiving and manuscript policies are encouraged to visit:

<http://www.elsevier.com/copyright>



Contents lists available at SciVerse ScienceDirect

## Journal of Non-Crystalline Solids

journal homepage: [www.elsevier.com/locate/jnoncrsol](http://www.elsevier.com/locate/jnoncrsol)

## Amorphous iron-chromium oxide nanoparticles prepared by sonochemistry

Nguyen Dang Phu<sup>a</sup>, Trinh Xuan Sy<sup>a</sup>, Hoang Thanh Cao<sup>a</sup>, Nguyen Ngoc Dinh<sup>a</sup>, Le Van Thien<sup>b</sup>,  
Nguyen Minh Hieu<sup>a</sup>, Nguyen Hoang Nam<sup>a</sup>, Nguyen Hoang Hai<sup>a,\*</sup>

<sup>a</sup> Center for Materials Science, Faculty of Physics, VNU University of Science, 334 Nguyen Trai, Thanh Xuan, Hanoi, Vietnam

<sup>b</sup> Faculty of Environmental Science, VNU University of Science, 334 Nguyen Trai, Thanh Xuan, Hanoi, Vietnam

## ARTICLE INFO

## Article history:

Received 1 August 2011

Received in revised form 24 October 2011

Available online 22 November 2011

## Keywords:

Crystallization process;

Amorphous iron oxide;

Sonochemistry;

Phase transition;

Magnetic property

## ABSTRACT

Amorphous  $\text{Fe}_2\text{O}_3$  and  $\text{Fe}_{1.9}\text{Cr}_{0.1}\text{O}_3$  materials have been prepared by sonochemical method. X-ray diffraction patterns, transmission electron microscopy, Raman and infrared spectra, differential scanning calorimetry, Mössbauer and magnetic measurements revealed many interesting behaviors of the samples. Reaction to form the materials only occurred at the preparation temperatures of 70 °C or above. Upon heating, the sample prepared at 70 °C presented a strong ferromagnetic behavior due to the presence of the magnetite phase coexisting with the hematite phase whereas the samples prepared at higher temperatures presented only the existence of the hematite phase. Thermal analyses of the sample prepared at 80 °C revealed three exothermic peaks which were corresponding to the phase changes of dehydroxylation, crystallization of the maghemite phase and maghemite–hematite transition, respectively. The activation energies of the phase changes deduced from the thermal analyses showed that the presence of Cr enhanced the activation energy which can slow down the ageing effect of the amorphous state when being used in practice.

© 2011 Elsevier B.V. All rights reserved.

## 1. Introduction

Amorphous metal oxides show great potentials in solar energy transformation [1,2], electronics [3], electrochemistry [4], manufacture of magnetic storage media, adsorption and purification processes and catalysis [5,6]. Among those oxides, iron oxide nanoparticles play an important role due to its excellent catalytic activity and high specific surface area. Iron oxide nanoparticles in the amorphous state are more interesting than in the crystalline state when being used as a catalyst due to the dangling bonds and high surface area [6]. They have been used for hydrogen peroxide oxidation of ferulic acid in water [7], As(V) and Cr(VI) removal [8]; as a catalyst for oxidation of cyclohexane [5,6], photoelectrode and photocatalyst for splitting water into  $\text{H}_2$  and  $\text{O}_2$  [9]; for magneto-optical sensors and magnetic devices [10], humidity sensors [11].

Amorphous iron oxide nanoparticles have been prepared by electrochemical synthesis [12], microwave heating [13], sonochemistry [14] because these methods provide a high cooling rate to form amorphous state. The most common way to obtain amorphous iron oxide nanoparticles is sonochemical technique. The cooling rate of this technique can be more than ten million degrees per second [15]. Sonochemical routes lead to iron oxides rely on  $\text{Fe}(\text{CO})_5$  [16,17],  $\text{FeCl}_3$  [18],  $\text{Fe}(\text{NO}_3)_3$  [19],  $\text{Fe}(\text{OAc})_2$  [20],  $\text{Fe}(\text{OEt})_3$  [21] as precursors.

The crystalline iron (III) oxides can commonly be maghemite ( $\gamma\text{-Fe}_2\text{O}_3$ ) or hematite ( $\alpha\text{-Fe}_2\text{O}_3$ ). The maghemite is ferrimagnetic with the saturation magnetization of about 60 emu/g. The hematite is antiferromagnetic with the Néel temperature of 680 °C. At room temperature nano-hematite sometimes behaves like a weak ferromagnet with low saturation magnetization of few emu/g [22] or sometimes high saturation magnetization [23]. Origin of the ferromagnetic property of the hematite was ascribed to a large number of point defects, or disorders in the materials. The hematite possesses a corundum-type structure with the space group of  $R\bar{3}c$  [23]. A transition from the maghemite to the hematite phase ( $\gamma\text{-}\alpha$  transition) occurred at 400 °C in iron oxide nanoparticles prepared by gas evaporation method. For iron oxide nanoparticles prepared by wet chemical method, the temperature at which the  $\gamma\text{-}\alpha$  transition happened varied in the range of 300 – 500 °C depending on the preparation method. Origin of the temperature difference is yet unsolved [24]. Iron oxide can be in another ferrimagnetic form called magnetite  $\text{Fe}_3\text{O}_4$  with the saturation magnetization of 80 emu/g [25].

Amorphous iron oxide, a metastable material, does not have the long-range order characteristic of a crystal. It has some short-range order at atomic length scale due to the nature of chemical bonding. Under certain conditions, the amorphous state can be changed to the crystalline states in a so-called crystallization process through which the physical and chemical properties of the materials change. The crystallization process occurs at all temperatures with different rates. The crystallization temperature is actually the temperature at which the rate of the crystallization process is highest. Below the crystallization temperature, the rate is much slower which is normally

\* Corresponding author. Tel: +84 4 3558 2216; fax: +84 4 3858 9496.  
E-mail address: [nhhai@vnu.edu.vn](mailto:nhhai@vnu.edu.vn) (N.H. Hai).

ignored in experiments. However, for applications of amorphous iron oxide materials, we have to study the changes in physical and chemical properties with time, namely the ageing effect. There are few articles reporting on the crystallization process of the iron oxides at the temperature of about 300 °C [13] but the effects of the crystallization process on the morphological, chemical and physical properties were not well studied. Especially no article reported on how to slow down the ageing process when the materials are used in applications.

Crystallization and phase transition processes are solid state reactions. The most used model to understand solid state reaction is the  $n$ th order model [26] which supposes that the degree of reaction  $\alpha$  is determined from:

$$\frac{d\alpha}{dt} = K(1-\alpha)^n \quad (1)$$

with  $t$  is the time and  $n$  is the order of reaction. The rate constant  $K$  is given by the Boltzmann–Arrhenius equation:  $K = K_0 \exp\{-E_a/RT\}$ , where  $E_a$  is the activation energy for the reaction, which describes the overall reaction process,  $R$  is the gas constant,  $T$  is the temperature, and  $K_0$  is the frequency factor or the pre-exponential factor. Kissinger proposed a method to calculate the kinetics parameters of the reaction [27] by using the data obtained from differential scanning calorimetry (DSC). He assumed that the reaction rate  $d\alpha/dt$  reaches maximum at the reaction temperature ( $T_p$ ) where DSC curve displays a peak. By solving the equation  $d^2\alpha/dt^2 = 0$  at  $T = T_p$ , the Kissinger equation is presented by:

$$\ln \frac{\beta}{T_p^2} = -\frac{E_a}{RT_p} + \ln \frac{K_0 R}{E_a} \quad (2)$$

where  $\beta$  is the heating rate (°C/min or K/min). By plotting the experimental data  $\ln(\beta/T_p^2)$  as a function of  $(-1/T_p)$  and fitting to Eq. (2), the kinetics parameters can be obtained. Among the kinetics parameters, the activation energy is an important one. If value of  $E_a$  is low, the reaction easily occurs and vice versa.

This article presents the study on the ageing effect of amorphous iron oxide nanoparticles prepared by sonochemical technique and find a way to improve the stability of the amorphous state by introducing chromium. The results showed that the presence of chromium increases the activation energy of the material.

## 2. Experimental

In principle, sonochemical experiments applied in this article are similar to other reports [14] but the reaction solution is different. Typically, 80 ml solution in a 150 ml vessel containing 0.01 M ferric chloride  $\text{FeCl}_3 \cdot 6\text{H}_2\text{O}$  (Guangdong chemical, China), 1 wt.% polyethylene glycol 2000 (Merk), 1 M urea (Xilong chemical, China) was ultrasonicated by using a ultrasound emitter (Sonics VCX 750) with a power of 400 W, a frequency of 20 kHz for 4 h  $\text{Cr}(\text{NO}_3)_3 \cdot 9\text{H}_2\text{O}$  (Guangdong chemical, China) was added to the solution in order to have  $\text{Fe}_2\text{O}_3$  (iron oxide sample) and  $\text{Fe}_{1.9}\text{Cr}_{0.1}\text{O}_3$  (iron-chromium oxide sample). Temperature of the system was adjusted in the temperature range from 70 to 90 °C. After cooling to room temperature, amorphous materials were collected by using a centrifuge (Hettich Universal 320, 1160 rcf for 20 min), washed five times with distilled water and air-dried at 75 °C. The samples were annealed in a muffle furnace in air at temperature range from 200 to 600 °C for 30 min. The structure of the nanoparticles was analyzed by using a Bruker D5005 X-ray diffractometer (XRD). The morphology of the materials was examined by a JEM-1200 EX transmission electron microscope (TEM) working at an accelerating voltage of 80 kV. The chemical composition was determined by using an energy dispersion spectroscopy (EDS) in a JEOL 5410 LV scanning electron microscope. Magnetic measurements were conducted by using a DMS-880 sample vibrating

magnetometer (VSM) with a maximum magnetic field of 13.5 kOe. The thermal behavior was examined by a STD 2960 TA Instruments differential scanning calorimetry (DSC) over the temperature range of 25–600 °C with different heating rates of 10–30 °C/min in air. Raman spectra were conducted by a Renishaw InVia Micro Raman at room temperature. The samples were excited using the 632.8 nm line from a He–Ne laser with a power level of about 1 mW. Fourier transformed infrared (FTIR) spectra were recorded in the transmission mode on a Nicolet Impact 410 spectrometer. Mössbauer spectra were measured at room temperature in the standard transmission geometry, using a traditional constant acceleration signal spectrometer with a  $^{57}\text{Co}:\text{Rh}$  as the source. Hyperfine interaction parameters of the as-prepared and annealed samples were derived from the Mössbauer spectra using a least-squares fitting. Isomer shifts were relative to  $\alpha\text{-Fe}$  at room temperature.

## 3. Results

The XRD patterns of the iron oxide samples prepared at  $T_e = 70, 80$  and 90 °C before and after heating up to 600 °C in the magnetization measurements (as presented in Fig. 4) are given in Fig. 1. The high signals at low angles appeared in all curves are due to the amorphous nature of the glass substrate supporting the materials in the XRD measurements. All the as-prepared materials presented very similar results with the absence of diffraction peaks, which shows the amorphous structure of the as-prepared iron oxide particles. Upon annealing, the crystallization processes occurred. Only the hematite phase ( $\alpha\text{-Fe}_2\text{O}_3$ ; JCPDS # 73-2234) was formed in the samples with  $T_e = 80$  and 90 °C whereas the coexistence of the hematite and the magnetite ( $\text{Fe}_3\text{O}_4$ ; JCPDS # 79-0418) phases presented in the samples with  $T_e = 70$  °C. The XRD patterns of the iron oxide sample prepared at 80 °C before and after annealing at  $T_a = 220 - 600$  °C are given in Fig. 2. Increasing  $T_a$  from 220 to 400 °C, the crystallization process developed gradually which was presented by the weak and broad diffraction peaks at 33.2, 35.6 and 62.5° assigned to either the  $\alpha\text{-Fe}_2\text{O}_3$  or  $\gamma\text{-Fe}_2\text{O}_3$  structures. At higher annealing temperatures of 500 and 600 °C, only the peaks of the hematite phase appeared and increased with increasing  $T_a$ .

TEM images of the iron oxide sample prepared at 80 °C are given in Fig. 3. Particle size increased from 5 nm for the as-prepared sample (Fig. 3(a)) to 22 nm for the sample annealed at 600 °C for 15 min (Fig. 3(b)), which was due to the particle growth and agglomeration process. A similar phenomenon was observed for the samples prepared at 70 and 90 °C.

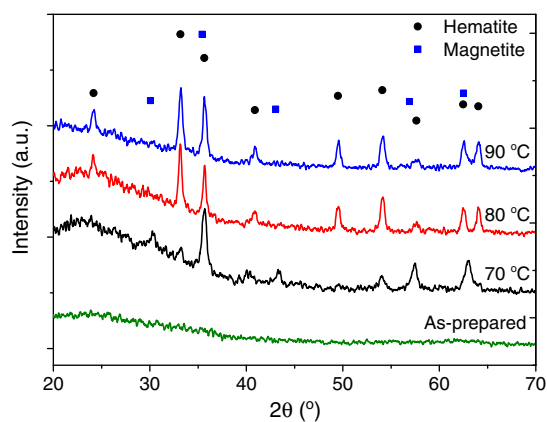
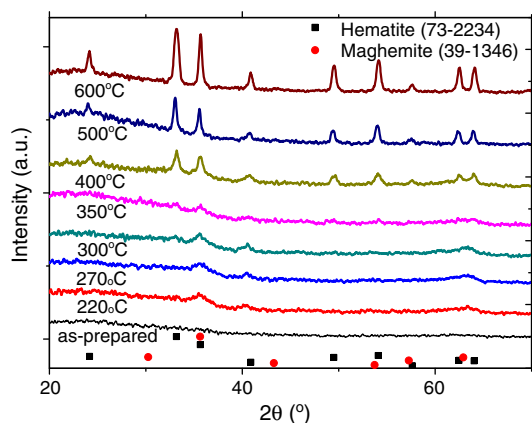


Fig. 1. XRD patterns of the iron oxide samples prepared at 70, 80 and 90 °C before (as-prepared) and after heating to 600 °C in the magnetization measurement as presented in Fig. 4. Most of the diffraction peaks are assigned to the hematite  $\text{Fe}_2\text{O}_3$  phase (JCPDS # 73-2234). Some peaks of the sample with  $T_e = 70$  °C may be assigned to the magnetite  $\text{Fe}_3\text{O}_4$  phase (JCPDS # 79-0418).



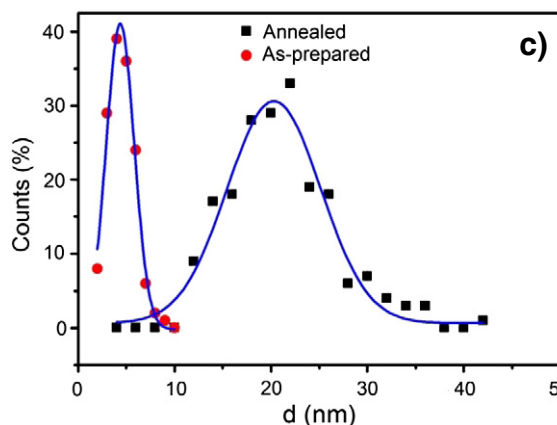
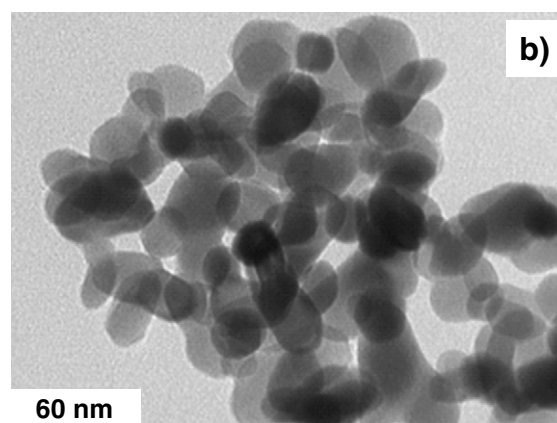
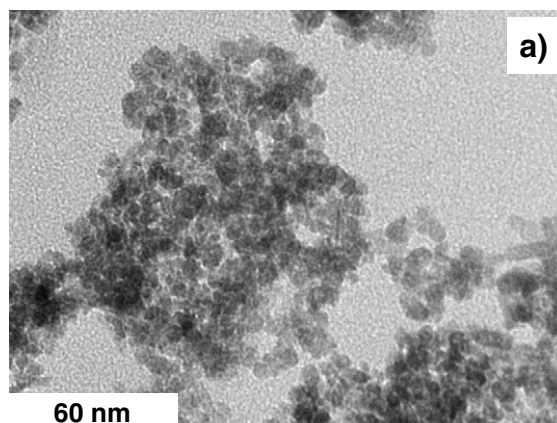
**Fig. 2.** XRD patterns of the sample prepared at 80 °C before and after annealing at 200–600 °C compared with the powder diffraction file of hematite (JCPDS # 73-2234) and maghemite (JCPDS # 39-1346).

Fig. 4 presents the temperature dependence of the magnetization under a magnetic field of 200 Oe for the iron oxide samples with  $T_e = 70, 80$  and 90 °C. All heating curves started with non-ferromagnetic state of the amorphous nature of the unannealed materials. At temperatures higher than 300 °C, the magnetization curves showed a strong enhancement which suggests that the crystallization process of a ferromagnetic phase occurred in the materials at those temperatures.

The heating curve of the sample with  $T_e = 70$  °C was higher, broader and more complicated than that of the two other samples with  $T_e = 80$  and 90 °C. There are two magnetic enhancements, the first one (strong) at 305 °C and the second one (weak) at 380 °C (Fig. 4(a)). The highest magnetization on the heating curve was 9 emu/g. At the temperatures of 600 °C and higher, the magnetization was almost zero due to the domination of thermal agitation over the magnetic exchange interaction appeared between the magnetic moments of Fe ions. The cooling curve started at 600 °C back to room temperature was a gradual and monotonic function as temperature and got a maximal value of 18 emu/g at room temperature. The heating and cooling curves of the amorphous iron oxide material prepared at 70 °C were similar to that of a typical ferromagnetic material [28]. The ferromagnetic property in this sample was supported by the fact that the magnetic field dependence of the magnetization at room temperature of the sample after cooling was hysteresis with the coercive field of 170 Oe and the saturation magnetization of 26 emu/g (Fig. 5).

The samples with  $T_e = 80$  and 90 °C presented heating curves with a single magnetic enhancement at about 370–380 °C (close to the second enhancement of the sample with  $T_e = 70$  °C which may be assigned to the formation of the maghemite phase) as shown in Fig. 4(a), (b). The highest value of the magnetization in the heating curve was about 1 emu/g, much lower than the value of the sample with  $T_e = 70$  °C. Moreover, the shape and value of the magnetization on the cooling curve of those samples revealed a non-ferromagnetic property.

The room temperature Mössbauer spectra of the as-prepared and annealed samples with  $T_e = 80$  °C are shown in Fig. 6. It can be seen that the spectrum of the as-prepared sample shows one doublet with isomer shift of 0.35 mm/s and quadrupole splitting of 0.66 mm/s. These values are quite similar to those reported for amorphous iron oxide materials [29], which are attributed to  $Fe^{3+}$  in the high-spin state. This implies that the as-prepared sample was paramagnetic. Spectrum of the sample annealed at 600 °C is different with the presence of one sextet. The fitting gave the hyperfine field of 512.6 kOe, isomer shift of 0.34 mm/s relative to  $\alpha$ -Fe. These parameters are in good agreement with those reported in the literatures for the hematite phase [6,30]. The



**Fig. 3.** TEM images of the as-prepared (a) and annealed at 600 °C (b) iron oxide nanoparticles with  $T_e = 80$  °C and fitting the particle size distribution to the Gaussian function (c).

contribution of doublet is only 2%. From these values, it is clear that the annealed samples mainly consist of  $\alpha$ - $Fe_2O_3$  hematite phase with anti-ferromagnetic order.

Fig. 7 presents the FTIR spectra of the iron oxide sample before and after annealing at 220–600 °C. All curves show a broad absorption band at around  $3400\text{ cm}^{-1}$  which was due to the H–OH stretch. The intensity of this band reduced with increasing  $T_a$ . Two adsorption bands which can be assigned to the hematite phase located at 450 and  $540\text{ cm}^{-1}$  [31] are clearly appeared in the sample annealed at 500 and 600 °C. This is another evidence for the presence of the hematite phase in the samples annealed at high temperatures. The presence of a band at  $690\text{ cm}^{-1}$  which disappeared in the sample annealed at 600 °C was assigned to tetrahedral defects [32].

Raman spectra of the iron oxide samples with  $T_e = 70, 80, 90$  °C after annealing at 600 °C are shown in Fig. 8. For the samples with

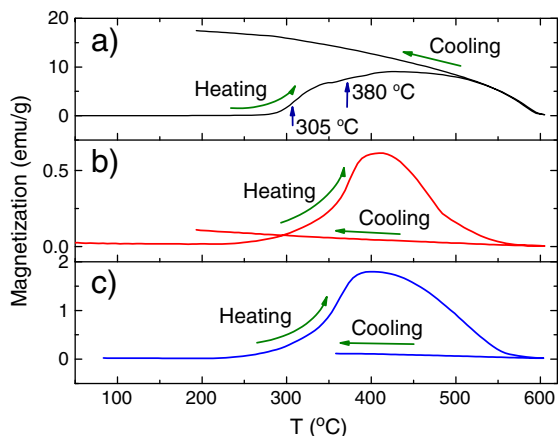


Fig. 4. Temperature dependence of the magnetization under the applied magnetic field of 200 Oe of the iron oxide nanoparticles with the preparation temperature of 70 °C (a), 80 °C (b) and 90 °C (c).

$T_e = 80$  and  $90$  °C, most of the peaks can be assigned to the hematite phase [33]:  $A_{1g}$  ( $225, 494 \text{ cm}^{-1}$ ),  $E_g$  ( $244, 290, 297, 409, 612 \text{ cm}^{-1}$ ) and second harmonic vibration ( $1320 \text{ cm}^{-1}$ ). The peak at  $660 \text{ cm}^{-1}$  which was very weak and sometimes ignored in other Ref. [33–35] is strong in this study. Some works [36,37] attributed this peak to the disorder-induced breaking of the symmetry properties of the  $E_u(\text{LO})$  phonon which may be caused by the defects in the materials. The disorders may come from a strong resonance on the surface of the nanoparticles, and the structural defects [38] formed due to the fast cooling in the preparation process. It can be seen that, the Raman spectra of the sample with  $T_e = 70$  °C shows a broad scattering band at  $685 \text{ cm}^{-1}$  (instead of two distinguished bands at  $610$  and  $660 \text{ cm}^{-1}$ ), indicating the formation of the magnetite phase [39]. The presence of a peak located at  $1590 \text{ cm}^{-1}$  is unknown to us and never reported in literature. Raman spectra of the iron oxide samples with  $T_e = 80$  °C after annealing at  $220$ – $600$  °C are shown in Fig. 9. When  $T_a \leq 270$  °C, the Raman spectra are similar to that of the un-annealed sample with a broad scattering band located at  $650$ – $750 \text{ cm}^{-1}$ . This band can be ascribed to the Fe–O symmetric stretch which presented in the amorphous state of the samples. This band appeared in many types of crystalline iron oxides such as goethite, magnetite, maghemite but not hematite phase [40,41,39]. At higher annealing temperatures of  $300$  and  $400$  °C, beside that broad scattering band, there were vague bands which are ascribed to the hematite

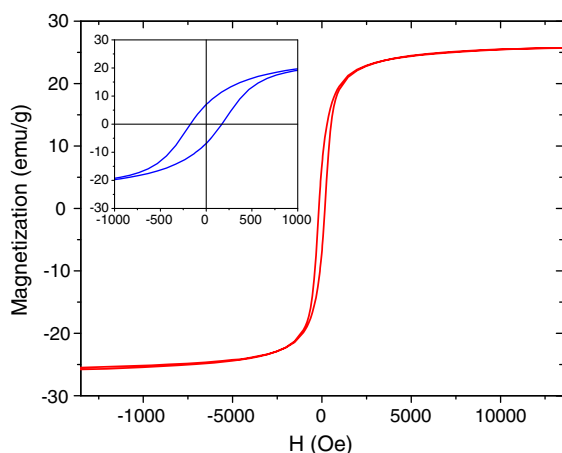


Fig. 5. Magnetic field dependence of the magnetization at room temperature of the sample with  $T_e = 70$  °C after heating–cooling magnetization measurement as showed in Fig. 4(a). The hysteresis loop presented a ferromagnetic property of the material. The inset is a zoom-in of the main figure.

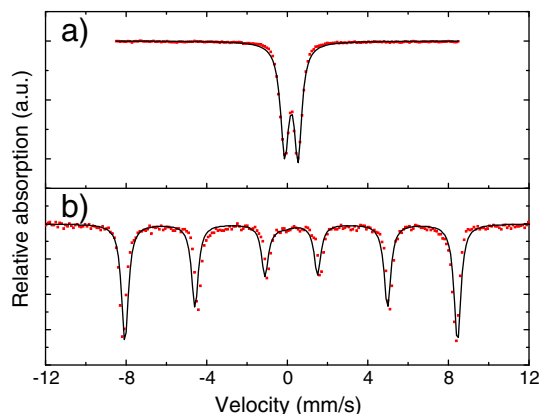


Fig. 6. Room temperature Mössbauer spectra of the as-prepared (a) and annealed at  $600$  °C (b) samples with  $T_e = 80$  °C.

phase. The intensity of these bands increased with increasing annealing time. At  $T_a = 500, 600$  °C the peak at  $650$ – $750 \text{ cm}^{-1}$  (assigned for the Fe–O symmetric stretch appeared in the amorphous state) completely disappeared and there were only the peaks presented for the hematite phase:  $A_{1g}$  ( $225, 494 \text{ cm}^{-1}$ ),  $E_g$  ( $244, 290, 297, 409, 612 \text{ cm}^{-1}$ ) and second harmonic vibration ( $1320 \text{ cm}^{-1}$ ).

DSC results of the iron oxide nanoparticles prepared at  $80$  °C with the heating rate of  $10$ – $30$  °C/min are given in Fig. 10. A part from an endothermic peak in the temperature range from  $25$  to  $180$  °C due to the evaporation of moieties in the samples (not shown), there are three obvious exothermic peaks located at around  $T_{p1} = 215$ ,  $T_{p2} = 265$  and  $T_{p3} = 505$  °C corresponding to the heating rate  $\beta = 10$  °C/min. All peaks have a tendency of shifting to higher temperatures as increasing the heating rate. According to Eq. (2), the activation energies of  $105, 130$  and  $186 \text{ kJ/mol}$  for the solid state reactions corresponding to the three exothermic peaks  $T_{p1}$ ,  $T_{p2}$  and  $T_{p3}$  were respectively deduced by fitting to the experimental DSC data (Table 1).

Chromium ions have been used to replace iron ions in its lattice positions as their ionic radii are of same order [44]. In addition, the structure of chromium oxide and the hematite phase of iron oxide are rhombohedral [45] and they are both antiferromagnetic insulator [46]. We study effects of the presence of Cr on the crystallization process. Concentration of  $\text{Cr}^{3+}$  was adjusted to have  $\text{Fe}_{1.9}\text{Cr}_{0.1}\text{O}_3$ . The experimental concentration of Cr in the as-prepared iron-chromium oxide sample obtained from EDS was  $0.098$  which was very close to the expected value of  $0.1$ . The lattice parameters ( $a = 5.045 \text{ \AA}$  and

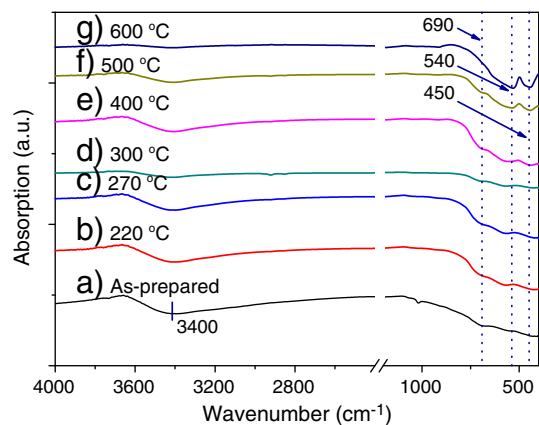


Fig. 7. FTIR spectra of the iron oxide samples with  $T_e = 80$  °C before and after annealing at  $220$ – $600$  °C.

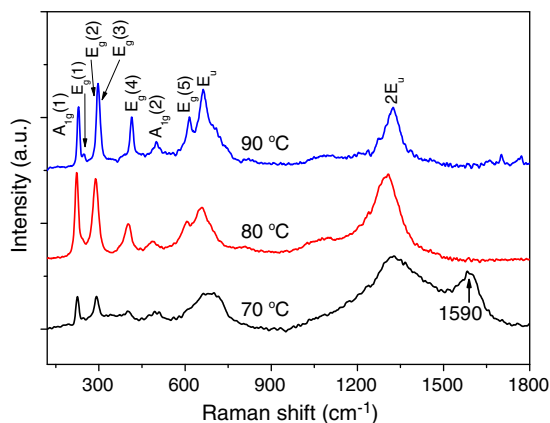


Fig. 8. Raman spectra of the iron oxide samples prepared at 70, 80 and 90 °C after heating to 600 °C in the magnetization measurement as presented in Fig. 4.

$c = 13.069 \text{ \AA}$ ) of the corundum-type structure of the hematite phase in the iron oxide are almost the same as the values for the iron-chromium oxide samples ( $a = 5.039 \text{ \AA}$  and  $c = 13.065 \text{ \AA}$ ). DSC data of the  $\text{Fe}_{1.9}\text{Cr}_{0.1}\text{O}_3$  sample with the heating rates of 10–30 K/min (the same heating rates applied for the amorphous iron oxide sample) are given in Table 2. All peaks have been shifted to higher temperatures compared to those of the iron oxide sample. The activation energies relatively corresponding to  $T_{p1}$ ,  $T_{p2}$  and  $T_{p3}$  are 140, 156, 170 kJ/mol.

Fig. 11 presents the time dependence of the magnetization of  $\text{Fe}_{1.9}\text{Cr}_{0.1}\text{O}_3$  at several temperatures around  $T_{p2} = 299 \text{ }^\circ\text{C}$ . All curves show a strong increase in magnetization for a short period of time after increasing the sample temperature. The trend was kept for the samples at 365 °C and below whereas at 395 and 420 °C the magnetization got a maximal value and reduced after about 600 s.

#### 4. Discussion

Formation of the amorphous nanoparticles in the preparation process may be explained in a similar way to form the amorphous iron oxide nanoparticles prepared by microwave heating technique [13]. Hydrated  $\text{Fe}(\text{Cr})^{3+}$  can form complexes with water molecules or  $\text{OH}^-$  ions to form  $\text{Fe}(\text{Cr})(\text{H}_2\text{O})_x(\text{OH}^-)_y^{(3-y)+}$ . Polymer of this hydroxide played a role of precursors for the oxide. The fast heating of the ultrasonic waves stimulated nucleation of iron oxide. With the simultaneous nucleation and homogeneous heating, uniformly small particles could be synthesized. Polyethylene glycol, as a dispersion stabilizer, inhibited non-homogeneous precipitation to obtain homogeneous precipitation. The pH of the solution was adjusted by

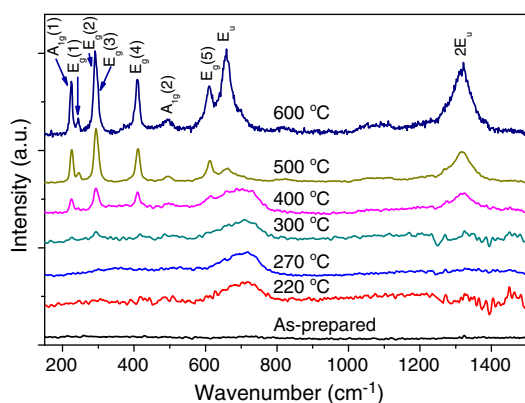


Fig. 9. Raman spectra of the iron oxide samples with  $T_e = 80 \text{ }^\circ\text{C}$  before and after annealing at 220–600 °C.

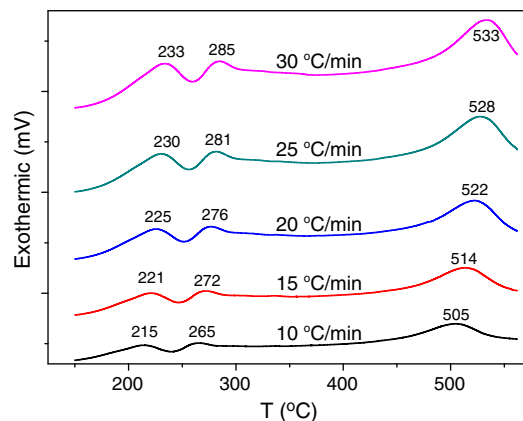


Fig. 10. DSC data of the iron oxide sample prepared at  $T_e = 80 \text{ }^\circ\text{C}$  with the heating rate of 10–30 °C/min.

hydrolysis urea, which was favorable for hydrolysis  $\text{Fe}(\text{Cr})^{3+}$  reaction. The temperature of the reaction solution is important for the preparation process. Nanoparticles could only be obtained at the experiment temperature  $T_e$  of 70, 80 and 90 °C. Below 70 °C, the reaction did not occur which may be explained by the formation of the hydroxide polymers at high temperatures.

Ferromagnetic property is the result of the exchange interaction appeared between magnetic moments aligned in crystalline structure with long-ranged order. In the amorphous iron oxide materials, even the magnetic moment of the Fe ions were present but the short-ranged order did not provide the exchange interaction. So that there was no ferromagnetic behavior appeared in the amorphous state at low temperatures of the heating curves (Fig. 4).

For the sample with  $T_e = 70 \text{ }^\circ\text{C}$ , we supposed that the amorphous nanoparticles were undergone two crystallization processes, i.e., the formation of the magnetite phase at 305 °C and the maghemite at 380 °C. Then the maghemite phase was changed to the hematite phase at 530 °C. That explained the two enhancements in the heating curve (Fig. 4(a)) and the presence of the magnetite phase in the XRD data (Fig. 1). At room temperature, the hematite phase is antiferromagnetic or weakly ferromagnetic therefore the strong ferromagnetic property of the sample was due to the magnetite phase (Fig. 5).

For the sample with  $T_e = 80$  and 90 °C, we supposed that the amorphous nanoparticles were undergone one crystallization processes, i.e., the formation of the hematite at 380 °C (at which the formation of the maghemite occurred in the sample with  $T_e = 70 \text{ }^\circ\text{C}$ ). Then the hematite phase was changed to the hematite phase at 530 °C. There was no presence of the magnetite phase in those samples. The ferromagnetic property shown on the heating curve in Fig. 4(b, c) was assigned to the maghemite phase. The XRD data also presented only the existence of the maghemite and hematite diffractions (Fig. 2). Non-ferromagnetic property of the samples shown

Table 1

Parameters related to the Kissinger plot (Eq. (2)) of the iron oxide sample,  $\beta$  ( $^\circ\text{C}/\text{min}$ ) is the heating rate,  $R_c^2$  is the correlation coefficient. Errors in the table were from the fitting to Eq. (2).

Parameters	$T_{p1}$ ( $^\circ\text{C}$ )	$T_{p2}$ ( $^\circ\text{C}$ )	$T_{p3}$ ( $^\circ\text{C}$ )
$\beta = 10$	215	265	505
$\beta = 15$	221	272	514
$\beta = 20$	225	276	522
$\beta = 25$	230	281	528
$\beta = 30$	233	285	533
$\ln \frac{KR}{E_a}$	$16.0 \pm 1.2$	$18.7 \pm 1.3$	$17.8 \pm 2.0$
$R_c^2$ (%)	99.1	99.1	98.0
$\frac{E_a}{R}$ ( $\times 10^3$ )	$12.7 \pm 0.6$	$15.6 \pm 0.7$	$22.4 \pm 1.6$
$E_a$ ( $\text{kJ} \cdot \text{mol}^{-1}$ )	$105 \pm 6$	$130 \pm 6$	$186 \pm 13$

**Table 2**

Parameters related to the Kissinger plot (Eq. (2)) of the  $\text{Fe}_{1.9}\text{Cr}_{0.1}\text{O}_3$  sample,  $\beta$  ( $^{\circ}\text{C}/\text{min}$ ) is the heating rate,  $R_c^2$  is the correlation coefficient. Errors in the table were from the fitting to Eq. (2).

Parameters	$T_{p1}$ ( $^{\circ}\text{C}$ )	$T_{p2}$ ( $^{\circ}\text{C}$ )	$T_{p3}$ ( $^{\circ}\text{C}$ )
$\beta = 10$	241	282	542
$\beta = 15$	245	289	551
$\beta = 20$	251	294	559
$\beta = 25$	253	297	563
$\beta = 30$	257	299	577
$\ln \frac{K_R}{E_a}$	$23.5 \pm 2.8$	$23.8 \pm 1.9$	$14.2 \pm 3.8$
$R_c^2$ (%)	97.2	98.9	91.0
$\frac{E_a}{R}$ ( $\times 10^3$ )	$17.3 \pm 1.5$	$18.9 \pm 1.0$	$20.5 \pm 3.1$
$E_a$ ( $\text{kJ} \cdot \text{mol}^{-1}$ )	$140 \pm 10$	$156 \pm 8$	$170 \pm 20$

on the cooling curve (Fig. 4(b) and (c)) was due to the hematite phase. The formation of the hematite phase was via the  $\gamma - \alpha$  transition where the ferromagnetic maghemite was changed to the antiferromagnetic hematite phase at high temperatures (as shown in the DSC data, Fig. 10).

The shifts of DSC peaks with heating rates of the sample with  $T_e = 80$   $^{\circ}\text{C}$  (Fig. 10) were the result of the fact that the samples have low thermal conductivity, therefore the temperature of the material in the center of the samples lagged the temperature on the surface. The value of the temperature lag increased with heating rate and made the solid state reaction be shifted to higher temperatures. Moreover, the solid state reaction is related to the change in molecular mobility, and this mobility has a small time-dependent or kinetic contribution. Combining with the XRD data (Fig. 2) and the magnetic measurements (Fig. 4), we supposed that the first peak is related to the dehydroxylation of the materials [42,43], the second exothermic peak is due to the crystallization process of the maghemite phase in the sample with  $T_e = 80$   $^{\circ}\text{C}$ . The maghemite possesses a strong ferromagnetic property which led to the enhancement in magnetization as shown in Fig. 4(b). The third exothermic peak is corresponding to the transition from the maghemite to the hematite phase ( $\gamma - \alpha$  transition). The hematite is antiferromagnetic therefore the magnetization of the cooling curve in Fig. 4(b) was low. Similar argument can be used to explain the magnetic results of the sample with  $T_e = 90$   $^{\circ}\text{C}$ . The dehydroxylation process occurred at  $T_{p1}$  did not affect strongly to the magnetic properties however the crystallization process of the maghemite phase at  $T_{p2}$  enhanced the magnetization in the materials. In contrast, the  $\gamma - \alpha$  transition reduced the magnetization. We studied the dynamics of the magnetization as a function of time (Fig. 11). The continuous increase in the magnetization at 305, 335 and 365  $^{\circ}\text{C}$  can be understood by the development of the maghemite phase at temperatures higher than the crystallization temperature  $T_{p2}$ . The reduction in the magnetization at 395 and 420  $^{\circ}\text{C}$  after 600 s can be explained by two processes: the development of the maghemite phase (enhancement in the magnetization) and the  $\gamma - \alpha$  transition (reduction in the magnetization). Even the measuring temperatures of 395 and 420  $^{\circ}\text{C}$  were lower than the transition temperature  $T_{p3}$  but the transition rates were much faster than that at 305, 335 and 365  $^{\circ}\text{C}$ . After the formation of the maghemite phase completed, the  $\gamma - \alpha$  transition dominated, which caused a reduction in the magnetization after long time.

For practical applications, the enhancement of  $T_{p1}$  and the activation energy corresponding to  $T_{p1}$  in the iron-chromium oxide compared to those of the iron oxide are important which leads to the fact that the amorphous state of the materials is more stable at room temperature. To estimate the life time of amorphous materials under a certain temperature, we take integration of Eq. (1):  $\int (1 - \alpha)^{-n} d\alpha = \int K_0 \exp\{-E_a/RT\} dt$ . The time for completing the reaction  $t \propto \exp\{E_a/RT\}$ . The reaction occurs at all temperatures with different rates. But at  $T_{p1}$  the reaction rate is much faster than at room temperature  $T_r$ . If the time periods for completing the reaction at  $T_{p1}$  and  $T_r$

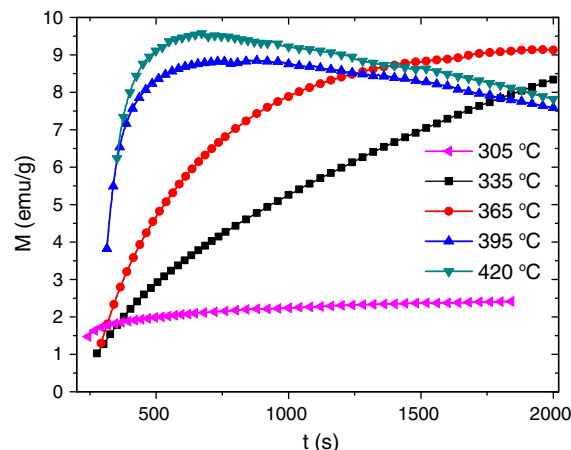


**Fig. 11.** Time dependence of the magnetization of the  $\text{Fe}_{1.9}\text{Cr}_{0.1}\text{O}_3$  with  $T_e = 80$   $^{\circ}\text{C}$  at different temperatures.

respectively are  $t_{T_{p1}}$  and  $t_r$ , supposing that the activation energy  $E_a$  is the same at different temperatures, we obtain  $t_r/t_{T_{p1}} \propto \exp\{E_a/RT_r\}/\exp\{E_a/RT_{p1}\}$ . Using the data for the iron oxide sample in Table 1 ( $T_{p1} \approx 225$   $^{\circ}\text{C}$ ,  $T_r \approx 27$   $^{\circ}\text{C}$ ,  $t_r/t_{T_{p1}} \approx 1.2 \times 10^7$ ,  $t_{T_{p1}}$  is about few seconds) we obtain  $t_r$  is about a year. Using data for the iron-chromium oxide sample in Table 2,  $t_r$  can be up to 15 years. Therefore, the presence of Cr can slow down the ageing effect by a factor of 15 times. This is a good way for using the amorphous iron-chromium oxide materials in practice.

## 5. Conclusion

Amorphous iron-chromium oxide materials have been prepared by sonochemistry. The crystallization and phase transition processes revealed that the formation of the maghemite and hematite started at 215  $^{\circ}\text{C}$  therefore the life time of the amorphous materials was limited under a year. Ageing effect of the amorphous iron oxide materials can be slowed down by the presence of Cr. It should be important when using the materials for practical applications.

## Acknowledgements

This work was financially supported by the National Foundation of Science and Technology Development (NAFOSTED Grant No. 103.02.68.09) and the key project QGTD.10.29 of Vietnam National University, Hanoi. Authors would like to thank Prof. O. M. Lemine of Imam University and Prof. M. Sieddine of Universite Sultan Moulay Slimane for the experimental helps.

## References

- [1] L. Machala, R. Zboril, A. Gedanken, J. Phys. Chem. B 111 (2007) 4003–4018.
- [2] B. Danzfuß, U. Stimming, J. Electroanal. Chem. 164 (1984) 89–119.
- [3] L. Murawski, C. Chung, J. Mackenzie, J. Non-Cryst. Solids 32 (1979) 91–104.
- [4] J. Sarradin, A. Guessous, M. Ribes, J. Power Sources 62 (1996) 149–154.
- [5] N. Perkas, Y. Koltypin, O. Palchik, A. Gedanken, S. Chandrasekaran, Appl. Catal., A 209 (2001) 125–130.
- [6] D.N. Srivastava, N. Perkas, A. Gedanken, I. Felner, J. Phys. Chem. B 106 (2002) 1878–1883.
- [7] R. Andreozzi, M. Canterino, V. Caprio, I.D. Somma, R. Marotta, J. Hazard. Mater. 152 (2008) 870–875.
- [8] M. Muruganandham, R. Amutha, B. Ahmmad, E. Repo, M. Sillanpaa, J. Phys. Chem. C 114 (2010) 22493–22501.
- [9] P.-S. Li, H. Teng, J. Chin. Inst. Chem. Eng. 38 (2007) 267–273.
- [10] L. Casas, A. Roig, E. RodrÁ-guez, E. Molins, J. Tejada, J. Sort, J. Non-Cryst. Solids 285 (2001) 37–43.
- [11] G. Neri, A. Bonavita, C. Milone, A. Pistone, S. Galvagno, Sens. Actuators, B 92 (2003) 326–330.
- [12] C. Pascal, J.L. Pascal, F. Favier, M.L. Elidrisi Moubtassim, C. Payen, Chem. Mater. 11 (1999) 141–147.
- [13] X. Liao, J. Zhu, W. Zhong, H.-Y. Chen, Mater. Lett. 50 (2001) 341–346.

- [14] J. Pinkas, V. Reichlova, R. Zboril, Z. Moravec, P. Bezdicka, J. Matejkova, *Ultrason. Sonochem.* 15 (2008) 257–264.
- [15] K.S. Suslick, S.-B. Choe, A.A. Cichowlas, M.W. Grinstaff, *Nature* 353 (1991) 414–416.
- [16] X. Cao, R. Prozorov, Y. Koltypin, G. Kataby, I. Felner, A. Gedanken, *J. Mater. Res.* 12 (1997) 402–406.
- [17] X. Cao, Y. Koltypin, R. Prozorov, G. Kataby, A. Gedanken, *J. Mater. Chem.* 7 (1997) 2447–2451.
- [18] W. Huang, X. Tang, I. Felner, Y. Koltypin, A. Gedanken, *Mater. Res. Bull.* 37 (2002) 1721–1735.
- [19] H. Schmidt, *Appl. Organomet. Chem.* 15 (2001) 331–343.
- [20] R.V. Kumar, Y. Koltypin, X.N. Xu, Y. Yeshurun, A. Gedanken, I. Felner, *J. Appl. Phys.* 89 (2001) 6324–6328.
- [21] D.N. Srivastava, N. Perkas, A. Zaban, A. Gedanken, *Pure Appl. Chem.* 74 (2002) 1509–1517.
- [22] R. Ramesh, K. Ashok, G.M. Bhalero, S. Ponnusamy, C. Muthamizhchelvan, *Cryst. Res. Technol.* 45 (2010) 965–968.
- [23] J. Wu, S. Mao, Z.-G. Ye, Z. Xie, L. Zheng, *Appl. Mater. Interfaces* 2 (2010) 1561–1564.
- [24] O. Kido, Y. Higashino, K. Kamitsuji, M. Kurumada, T. Sato, Y. Kimura, H. Suzuki, Y. Saito, C. Kaito, *J. Phys. Soc. Jpn.* 73 (2004) 2014–2016.
- [25] N.D. Phu, P.C. Phong, N. Chau, N.H. Luong, L.H. Hoang, N.H. Hai, *J. Exp. Nanosci.* 4 (2009) 253–258.
- [26] J. Elder, *Thermochim. Acta* 243 (1994) 209–222.
- [27] H.E. Kissinger, *Anal. Chem.* 29 (1957) 1702–1706.
- [28] D.-T. Ngo, M.S. Mahmud, N.H. Hai, D.T.H. Gam, N.Q. Hoa, S. McVitie, N. Chau, *J. Magn. Mater.* 322 (2010) 342–347.
- [29] T. Prozorov, R. Prozorov, Y. Koltypin, I. Felner, A. Gedanken, *J. Phys. Chem. B* 102 (1998) 10165–10168.
- [30] O.M. Lemine, M. Sajieddine, M. Bououdina, R. Msalam, S. Mufti, A. Alyamani, *J. Alloys Compd.* 502 (2010) 279–282.
- [31] T. Osaka, T. Matsunaga, T. Nakanishi, A. Arakaki, D. Niwa, H. Iida, *Anal. Bioanal. Chem.* 384 (2006) 593–600.
- [32] I.V. Chernyshova, M.F. Hochella Jr., A.S. Madden, *Phys. Chem. Chem. Phys.* 9 (2007) 1736–1750.
- [33] S.-H. Shim, T.S. Duffy, *Am. Mineral.* 87 (2002) 318–326.
- [34] I.R. Beattie, T.R. Gilson, *J. Chem. Soc. A* (1970) 980–986.
- [35] M.J. Massey, U. Baier, R. Merlin, W.H. Weber, *Phys. Rev. B* 41 (1990) 7822–7827.
- [36] K.F. McCarty, *Solid State Commun.* 68 (1988) 799–802.
- [37] D. de Faria, F. Lopes, *Vib. Spectro.* 45 (2007) 117–121.
- [38] A.L. Schoenhalz, J.T. Arantes, A. Fazzio, G.M. Dalpian, *Appl. Phys. Lett.* 94 (2009) 162503–162505.
- [39] O.N. Shebanova, P. Lazor, *J. Raman Spectrosc.* 34 (2003) 845–852.
- [40] G. Nauer, P. Strecha, N. Brinda-Konopik, G. Liptay, *J. Therm. Anal. Calorim.* 30 (1985) 813–830.
- [41] D.L.A. de Faria, S. Venâncio Silva, M.T. de Oliveira, *J. Raman Spectrosc.* 28 (1997) 873–878.
- [42] B. Zhao, Y. Wang, H. Guo, J. Wang, Y. He, Z. Jiao, M. Wu, *Mater. Sci. Poland* 25 (2007) 1143.
- [43] T. Henmi, *Clay Clay Miner.* 28 (1980) 92–96.
- [44] H. Levinstein, M. Robbins, C. Capiro, *Mater. Res. Bull.* 7 (1972) 27–34.
- [45] Y.-Y. Li, *Phys. Rev.* 101 (1956) 1450–1454.
- [46] W.P. Osmond, *Proc. Phys. Soc.* 79 (1962) 394.